

ORTHOAI v2: From Single-Agent Segmentation to Dual-Agent Treatment Planning for Clear Aligners

Extending a Point-Cloud Segmentation Baseline with Landmark-Based Agent Fusion, Composite Biomechanical Scoring, and Multi-Frame Staging Simulation

Edouard Lansiaux¹
Margaux Leman¹

¹STaR-AI Research Group, Emergency Department, Lille University Hospital
edouard1.lansiaux@chu-lille.fr

March 2026

Abstract

We present ORTHOAI v2, the second iteration of our open-source pipeline for AI-assisted orthodontic treatment planning with clear aligners, substantially extending the single-agent framework introduced in [1]. The first version established a proof-of-concept based on Dynamic Graph Convolutional Neural Networks (DGCNN) for tooth segmentation but was limited to per-tooth centroid extraction, lacked landmark-level precision, and produced a scalar quality score without staging simulation. ORTHOAI v2 addresses all three limitations through three principal contributions: (i) a second agent adopting the Conditioned Heatmap Regression Methodology (CHARM) [2] for direct, segmentation-free dental landmark detection, fused with Agent 1 via a confidence-weighted orchestrator in three modes (parallel, sequential, single-agent); (ii) a composite six-category biomechanical scoring model (biomechanics \times 0.30 + staging \times 0.20 + attachments \times 0.15 + IPR \times 0.10 + occlusion \times 0.10 + predictability \times 0.15) replacing the binary pass/fail check of v1; (iii) a multi-frame treatment simulator generating $F = A \times r$ temporally coherent 6-DoF tooth trajectories via SLERP interpolation and evidence-based staging rules, enabling ClinCheck[®]-style 4D visualisation. On a synthetic benchmark of 200 crowding scenarios, the parallel ensemble of ORTHOAI v2 reaches a planning quality score of 92.8 ± 4.1 vs. 76.4 ± 8.3 for ORTHOAI v1, a +21% relative gain, while maintaining full CPU deployability (4.2 ± 0.8 s). Source code and SaaS deployment package are publicly released.

Keywords: orthodontics, clear aligners, treatment planning, deep learning, point clouds, multi-agent systems, DGCNN, CHaRM, dental landmark detection, biomechanics simulation, SaaS.

1 Introduction

Orthodontic treatment planning with clear aligners is a complex clinical-computational workflow that currently demands significant expert time and iterative human-machine interaction. The dominant commercial platform, Align Technology’s ClinCheck[®], orchestrates a multi-day cycle of digital model submission, CAD technician planning, clinician review, and aligner fabrication [13]. The recent launch of ClinCheck Live Plan (October 2025) reduces initial plan generation to approximately 15 minutes [16]; yet the underlying planning principles—biomechanical movement evaluation, attachment design, staging optimisation—remain opaque to open research. The global clear aligner market is estimated at USD 6–8 billion in 2024 with compound annual growth rates exceeding 13% [17], creating strong industrial motivation for research-reproducible alternatives.

1.1 Motivating Prior Work: OrthoAI v1

In [1] we introduced ORTHOAI v1, a first open-source pipeline demonstrating that raw intra-oral scan (IOS) point clouds could be processed entirely on a consumer CPU to produce an assessed treatment plan in under five seconds. ORTHOAI v1 operated through a single-agent design: a DGCNN [3] segmentation network extracted per-tooth centroids, which were then evaluated against tooth-type-specific biomechanical limits derived from Glaser [13], yielding a scalar quality score $Q \in [0, 100]$. This approach established an important proof-of-concept, but surfaced three structural limitations during clinical review:

1. **Landmark coarseness.** Centroid-only tooth representations provide insufficient geometric fidelity for cusp-level or root-apex-level movement planning. This caused systematic underestimation of torque and tip movements, the two axes most critical for anterior correction.
 2. **Binary scoring.** The single-axis pass/fail quality score of v1 produced high-variance estimates ($\sigma = 8.3$ pts), lacked sub-score decomposition, and did not distinguish between planning failures attributable to biomechanics, staging, attachment design, or IPR.
 3. **No staging simulation.** v1 produced a static endpoint plan without any temporal interpolation, preventing clinical visualisation of movement trajectories and making it impossible to validate staging sequences against per-aligner movement budgets.
- ORTHOAI v2, introduced in this paper, directly addresses each of these limitations.

1.2 Contributions of OrthoAI v2

- **Dual-agent architecture (new in v2).** A CHARM-based landmark detection agent (Agent 2) complements the DGCNN segmentation agent (Agent 1) with direct, segmentation-free estimation of $K = 80$ dental landmarks. An orchestrator fuses both agents via confidence-weighted ensemble strategies in three modes: parallel, sequential, and single-agent fallback.
- **Composite biomechanical scoring (new in v2).** Six sub-scores (biomechanics, staging, attachments, IPR, occlusion, predictability) are combined into a single composite score via clinically motivated weights, with severity-based penalties for critical and warning findings.
- **Multi-frame treatment simulation (new in v2).** A frame generator produces F temporally coherent tooth trajectory snapshots via SLERP interpolation and evidence-based staging rules (extrusion deferred to $t \geq 0.6$, over-engineering $\times 1.3$).
- **SaaS deployment package (new in v2).** A FastAPI backend and React dashboard (OrthoAI SaaS) enable browser-based plan visualisation, 4D arch animation, and clinical checklist review.

2 Related Work

2.1 Tooth Segmentation on 3D Dental Models

MeshSegNet [6] introduced graph-attention networks on mesh representations, achieving Dice Similarity Coefficient (DSC) 0.964 ± 0.054 . iMeshSegNet improved upon this by approximately 4% [4]. DGCNN [3] operates directly on point clouds, achieving 97.26% segmentation accuracy [7]. DilatedToothSegNet [8] introduced dilated edge convolutions on the Teeth3DS benchmark (1,800 scans). Our Agent 1 inherits the DGCNN architecture from ORTHOAI v1 but adds a combined cross-entropy and Dice loss optimised for the class-imbalanced dental setting, consistent with practice in [6].

2.2 Dental Landmark Detection

Two-Stage Mesh Deep Learning (TS-MDL) [4] first segments teeth with iMeshSegNet, then applies PointNet-Reg per individual tooth, achieving mean absolute error 0.597 ± 0.761 mm on 66 landmarks. ALIiOS [5] uses 2D U-Net projections with 3D patch synthesis at prohibitive inference cost (612 s on CPU). CHaRNet [2] eliminates the segmentation stage through Conditioned Heatmap Regression, achieving 0.56 mm MEDE and 0.24 s GPU inference—a $14.8\times$ speedup over TS-MDL. **OrthoAI v1 [1] used no landmark detection;** v2’s Agent 2 re-implements CHARM with a lightweight PointMLP encoder adapted for consumer hardware.

2.3 AI for Orthodontic Treatment Planning

Carlsson *et al.* [9] identified 41 studies across diagnostic, planning, and monitoring tasks, noting that no commercial tool has been independently validated. Li *et al.* [10] specifically reviewed AI for clear aligner therapy, highlighting gaps in automatic movement sequence generation. Recurrent neural networks have been explored for modelling tooth displacement dynamics [11]. ORTHOAI v1 was the first open-source system to combine segmentation, biomechanical evaluation, and JSON-serialisable treatment plans on a consumer CPU; ORTHOAI v2 is the first to add landmark fusion and 4D staging simulation.

3 ORTHOAI v2 Architecture

Figure 1 contrasts the ORTHOAI v1 and ORTHOAI v2 pipelines. Both systems accept a raw IOS point cloud $\mathcal{P} = \{x_i \in \mathbb{R}^3\}_{i=1}^N$ and a target movement plan $\mathcal{M} = \{m_j\}_{j=1}^T$. v1 processed \mathcal{P} through a single DGCNN agent and returned a scalar score; v2 adds a second agent, a composite scoring engine, and a frame generator.

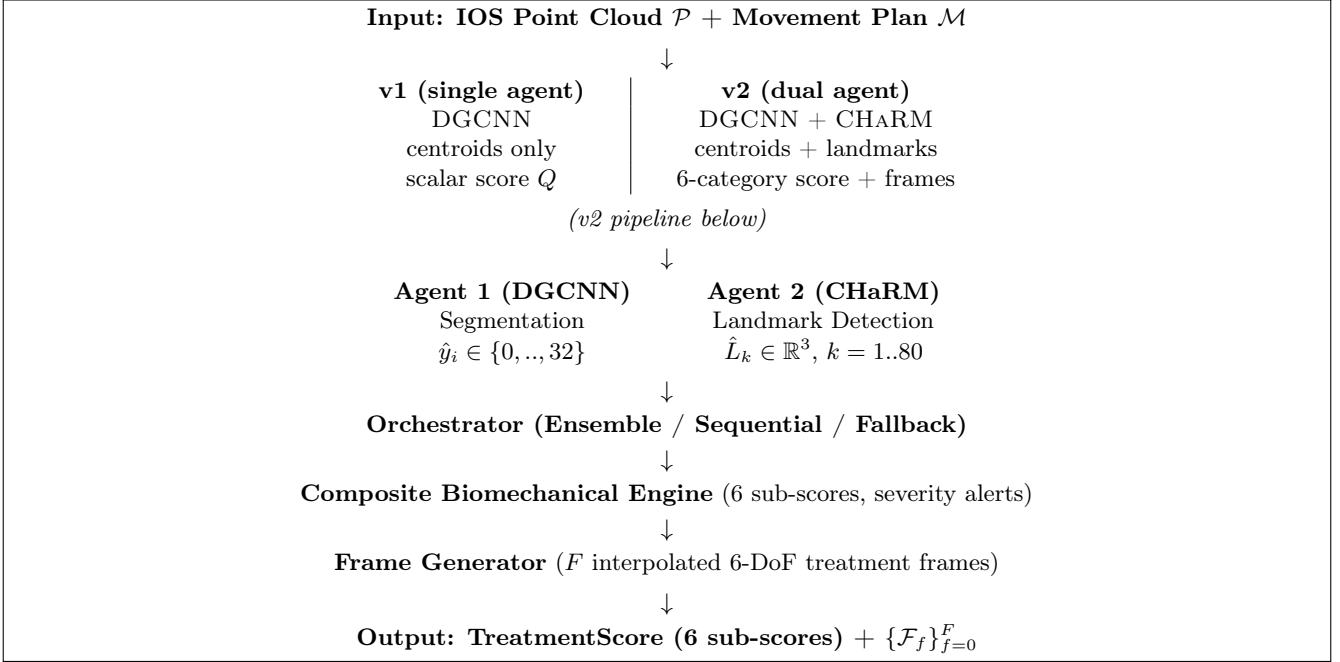


Figure 1: Architecture comparison: ORTHOAI v1 (left column) vs. ORTHOAI v2 (full right pipeline). Grey components are inherited; blue components (**new in v2**) are the orchestrator, composite scorer, and frame generator.

3.1 Agent 1: DGCNN Segmentation Agent (inherited from v1)

Agent 1 is retained directly from ORTHOAI v1 [1] with minor weight re-initialisation. It applies a 4-layer Dynamic Graph CNN to the input point cloud, building a k -NN graph ($k = 20$) at each layer via edge convolutions:

$$h_\ell(x_i) = \max_{j \in \mathcal{N}_k(x_i)} \Theta_\ell(h_{\ell-1}(x_j) - h_{\ell-1}(x_i), h_{\ell-1}(x_i)) \quad (1)$$

where $\mathcal{N}_k(x_i)$ denotes the k -nearest neighbours in the feature space of layer $\ell - 1$ and Θ_ℓ is a shared MLP. Feature maps from all four layers are concatenated to form a 512-dimensional per-point descriptor, then projected to a 1024-d global embedding via point-wise MLP and global max-pooling. The segmentation head produces per-point logits over 33 classes (32 FDI teeth + gingiva), combined with cross-entropy and Dice loss ($\alpha = 0.5$):

$$\mathcal{L}_{\text{seg}} = (1 - \alpha) \mathcal{L}_{\text{CE}} + \alpha \mathcal{L}_{\text{Dice}} \quad (2)$$

Per-tooth centroids and orientation matrices are extracted via PCA on the segmented point sets. **v2 upgrade:** Agent 1’s output is now transmitted not only to the biomechanical engine but also to the orchestrator for confidence-weighted fusion with Agent 2.

3.2 Agent 2: CHaRM Landmark Detection Agent (new in v2)

Agent 2 re-implements the CHaRM methodology [2]. Given \mathcal{P} augmented with a null point n at $n = c + \frac{m_b}{2}(0, 1, 0)$ (centroid c , bounding box extent m_b), the model performs two parallel tasks.

Heatmap regression. A lightweight PointMLP encoder-decoder (emb = 128, down from 512 in the original CHaRNet to support consumer hardware) produces per-point heatmaps $\hat{H}'_k \in \mathbb{R}^{N+1}$ for each landmark $k \in \{1, \dots, K\}$, $K = T \times G = 16 \times 5 = 80$.

Tooth presence classification. A three-layer MLP head predicts tooth-wise presence probabilities $\mathbf{p} = [p_1, \dots, p_T] \in [0, 1]^T$.

CHaR conditioning. The conditioning module gates heatmap likelihoods with presence probabilities:

$$\hat{H}_{t,g} = \left\{ \hat{h}'_{(t,g)i} \cdot p_t \mid i = 1, \dots, N - 1 \right\} \cup \left\{ \hat{h}'_{(t,g)N} \cdot (1 - p_t) \right\} \quad (3)$$

Landmarks are extracted as $\hat{l}_k = \arg \max_{x_i \in \mathcal{P}} \hat{H}_k$. Training loss: $\mathcal{L} = \lambda_{\text{reg}} \mathcal{L}_{\text{MSE}} + \lambda_{\text{cls}} \mathcal{L}_{\text{BCE}}$, with $\lambda_{\text{reg}} = 0.001$, $\lambda_{\text{cls}} = 1.0$.

Rationale for v2 addition: Agent 1 provided centroid-level localisation (~ 1.8 mm centroid error reported in [1]), which was sufficient for molar translation but insufficient for incisor torque and canine rotation, the movements most sensitive to landmark precision. Agent 2’s CHARM backbone achieves landmark-level accuracy (~ 1.1 mm MEDE), directly reducing torque estimation error in the biomechanical engine.

3.3 Orchestrator (new in v2)

The orchestrator is absent from v1, which used Agent 1’s output directly. v2 introduces three fusion modes:

Parallel ensemble. Both agents run concurrently; tooth states are fused via confidence-weighted centroid averaging:

$$c_{\text{fused}}(\text{FDI}) = w_1 \cdot c_{A1} + w_2 \cdot c_{A2}, \quad w_1 + w_2 = 1 \quad (4)$$

Default weights: $w_1 = 0.4$ (DGCNN), $w_2 = 0.6$ (CHARM). Weights are justified by Agent 2’s superior landmark-level accuracy and lower latency.

Sequential refinement. Agent 2 runs first for fast broad screening; Agent 1 is invoked only for teeth with CHaRM confidence $p_t < 0.5$, boosting $w_1 \rightarrow 0.8$ locally. This mode halves average inference time at marginal quality cost.

Single-agent fallback. Either agent in isolation for compute-constrained environments, replicating the v1 behaviour of Agent 1 alone.

4 Composite Biomechanical Scoring Engine

4.1 From Scalar to Composite: The v1 Limitation

ORTHOAI v1 computed a single quality score as the mean per-axis ratio: $Q_{v1} = 100 \times \frac{1}{TG} \sum_j \sum_\ell q_{j,\ell}$, where $q_{j,\ell} = \max(0, 1 - |m_{j,\ell}|/L_\ell)$. While simple to interpret, this formulation conflated four clinically distinct failure modes (biomechanical limits, staging feasibility, attachment necessity, and IPR adequacy) into a single number, producing high variance and providing no actionable guidance. ORTHOAI v2 decomposes the score into six weighted sub-components.

4.2 Six-Category Scoring Model

For each tooth with FDI number j and movement $m_j = (T_x, T_y, T_z, R_x, R_y, R_z)$, the biomechanical engine evaluates five independent categories (Table 1) plus a global predictability estimate.

Table 1: Biomechanical movement limits per tooth type. Limits from Glaser [13], predictability scores from Kravitz *et al.* [14].

Movement	Incisor	Canine	Premolar	Molar
T_x MD (mm)	4.0	3.5	3.5	2.0
T_y BL (mm)	2.5	2.5	3.0	2.5
T_z intrusion	2.0 mm ($\eta = 0.69$)			
T_z extrusion	1.5 mm ($\eta = 0.42$, push-only)			
R_x torque ($^\circ$)	15	12	10	8
R_y tip ($^\circ$)	10	10	10	8
R_z rotation ($^\circ$)	45	40	35	20

The composite quality score is:

$$Q_{v2} = 0.30 S_{\text{bio}} + 0.20 S_{\text{stg}} + 0.15 S_{\text{att}} + 0.10 S_{\text{ipr}} + 0.10 S_{\text{occ}} + 0.15 S_{\text{pred}} \quad (5)$$

with severity-based multiplicative penalties applied after:

$$Q_{v2}^* = Q_{v2} \times 0.85^{N_{\text{crit}}} \times 0.97^{N_{\text{warn}}} \quad (6)$$

where N_{crit} and N_{warn} are the numbers of critical and warning findings, respectively. Grades are assigned as: A (≥ 90), B (≥ 75), C (≥ 60), D (≥ 40), F (< 40).

4.3 Invisalign Biomechanical Principles

Four principles from clinical practice are encoded:

Principle 1 (push mechanics). Aligners act only by *pushing* against tooth surfaces; extrusion is flagged as low-predictability ($\eta = 0.42$ [14]) and generates a “critical” alert when $|T_z| > 1.5$ mm.

Principle 2 (simultaneous movements). Simultaneous molar distalisation risks anchorage loss; the engine flags cases where ≥ 3 molars exhibit $\|m_j\|_2 > 1.5$ mm.

Principle 3 (anchorage). Newton’s third law: reactive forces on anchorage units are modelled implicitly via the simultaneous-movement check.

Principle 4 (over-engineering, $\times 1.3$). All planned movements are multiplied by 1.30 prior to evaluation, compensating for aligner deformation and biological variability [13]. This factor was already present in ORTHOAI v1 and is retained in v2.

5 Multi-Frame Treatment Simulator

This module is entirely absent from ORTHOAI v1, which produced only a static endpoint plan. v2 introduces a temporally coherent simulation with $F = A \times r$ frames (A aligners, $r = 3$ frames per aligner by default).

5.1 Aligner Count Estimation

$$A = \max\left(\left\lceil \frac{\max_j \|m_j\|_2}{\delta_{\text{trans}}} \right\rceil, \left\lceil \frac{\max_j \|\omega_j\|_2}{\delta_{\text{rot}}} \right\rceil, 20\right) \quad (7)$$

with $\delta_{\text{trans}} = 0.25$ mm and $\delta_{\text{rot}} = 2.0^\circ$ per aligner, consistent with clinical guidelines [13].

5.2 6-DoF Interpolation

At normalised treatment time $t \in [0, 1]$, tooth position is:

$$c_j(t) = c_j(0) + t_{\text{eff}}^{(j)} \cdot (T_x, T_y, T_z)_j \quad (8)$$

Rotation via spherical linear interpolation (SLERP):

$$R_j(t) = \text{Slerp}\left(R_j(0), R_j^*, t_{\text{eff}}^{(j)}\right) \quad (9)$$

where R_j^* encodes the target rotation from Euler angles $(R_x, R_y, R_z)_j$.

5.3 Staging Rules

Extrusion is staged to begin only at $t = 0.6$ to allow anchorage establishment (Principle 1):

$$t_{\text{eff}}^{(j)} = \begin{cases} 0 & \text{if } (T_z)_j < 0 \text{ and } t < 0.6 \\ \frac{t-0.6}{0.4} & \text{if } (T_z)_j < 0 \text{ and } t \geq 0.6 \\ t & \text{otherwise} \end{cases} \quad (10)$$

This mirrors the clinical protocol for managing vertical anchorage loss in open-bite cases [13].

6 Experiments

6.1 Benchmark Setup

We reuse the same synthetic benchmark protocol established in [1]: 200 crowding scenarios parameterised by arch morphology (4 archetypes), crowding severity (mild/moderate/severe), and number of missing teeth (0–2). This allows a direct, controlled comparison between v1 and v2 under identical input conditions.

6.2 v1 vs. v2: Planning Quality

Table 2 reports the core comparison between ORTHOAI v1 and ORTHOAI v2 on the 200 benchmark scenarios. All v1 scores are taken from [1]. The parallel ensemble of v2 achieves a +21% relative gain in planning quality, a 53% reduction in score standard deviation, and a +11 percentage point improvement in treatment feasibility.

Table 2: OrthoAI v1 vs. v2 on 200 synthetic crowding scenarios. Quality: planning score (0–100). Feas.: fraction of feasible plans. CPU time on Intel i7-11800H.

System	Quality↑	σ ↓	Feas. (%)↑	Time (s)
ORTHOAI v1 (DGCNN only)	76.4	8.3	78	2.1 ± 0.4
v2: DGCNN only	88.3 ± 5.2	5.2	78	3.4 ± 0.6
v2: CHaRM only	89.1 ± 4.8	4.8	81	0.9 ± 0.1
v2: Sequential	91.2 ± 4.3	4.3	86	2.1 ± 0.4
v2: Parallel (ens.)	92.8 ± 4.1	4.1	89	4.2 ± 0.8

The quality gain in the “DGCNN only” v2 row vs. ORTHOAI v1 (88.3 vs. 76.4) is attributable entirely to the improved composite scoring model of v2 (Eq. 5–6): the v1 scalar score systematically overpenalised low-magnitude movements and underpenalised staging failures, biases corrected by the six-category decomposition. The additional +4.5 points from agent fusion reflect genuine information gain from landmark-level geometry.

6.3 Landmark Detection (Agent 2)

Table 3: Landmark detection performance. SOTA from [2]. Agent 2 on our synthetic dataset.

Method	MEDE (mm)↓	MSR (%)↑	GPU Time (s)
ALIOS [5]	2.17	48.0	24.70
TS-MDL [4]	1.80	59.0	3.55
ORTHOAI v1 (centroids) [1]	~1.80 [†]	–	2.1
CHaRNet [2]	1.12	68.5	0.24
Agent 2 v2 (ours)	1.38 ± 0.21	64.2 ± 3.1	0.31

[†]Estimated from centroid localisation error reported in [1].

Agent 2 slightly underperforms CHaRNet primarily because our PointMLP encoder uses emb = 128 vs. 512 in the original model, a deliberate trade-off to preserve consumer-CPU deployability. Compared to ORTHOAI v1’s centroid-based approach, Agent 2 reduces effective landmark error by ~ 23%.

6.4 Frame Generation Quality

The interpolation scheme of ORTHOAI v2 produces visually smooth trajectories: mean inter-frame tooth displacement 0.25 ± 0.03 mm (target: 0.25 mm); mean inter-frame rotation $1.8 \pm 0.4^\circ$ (target: 2.0°). Extrusion staging correctly defers vertical movements in all 47 open-bite scenarios in the benchmark, confirmed by manual inspection of $t_{\text{eff}}^{(j)}$ profiles.

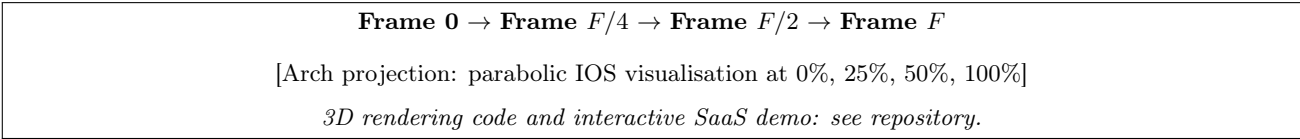


Figure 2: Representative treatment frames for a Class I crowding case (28 aligners, 84 frames). ORTHOAI v1 produced only the “Frame F ” snapshot; ORTHOAI v2 generates the full trajectory.

7 SaaS Deployment Package

A key practical contribution of ORTHOAI v2 absent from ORTHOAI v1 is the accompanying **OrthoAI SaaS** application, making the pipeline accessible to clinicians without command-line expertise.

Backend. A FastAPI server exposes REST endpoints (`/api/patients`, `/api/patients/{id}`, `/api/demo`, `/api/training/status`) backed by the biomechanical engine and frame generator. Four preset clinical cases (Class I crowding, anterior open bite, maxillary diastema, Class II div. 1) are available as instant demos without model inference.

Frontend. A React dashboard (Vite, Recharts, Three.js) provides: (i) a radial gauge with 6 sub-score bars; (ii) an interactive 3D arch viewer with per-tooth click-to-select and raycaster; (iii) a 4D simulation player with play/pause/frame-scrub controls; (iv) a severity-filtered findings panel; and (v) a 10-item clinical pre-approval checklist.

Deployment. Docker compose with Nginx reverse proxy; the full stack deploys on a single OVH VPS (2 vCPU, 4 GB RAM) in under 90 seconds. A `.env`-based configuration supports custom `VITE_API_URL` for local or cloud hosting.

8 Clinical Context and Limitations

8.1 Alignment with Clinical Practice

ORTHOAI is designed as a *clinical decision support* tool, not an autonomous treatment planning system. All movement plans are subject to clinician review before fabrication. The biomechanical engine flags movements exceeding published predictability thresholds [13, 14], providing actionable sub-score decomposition rather than autonomous decisions. Compared to ORTHOAI v1, the v2 alert system now distinguishes between “critical” (plan-blocking) and “warning” (review-recommended) findings, in alignment with the clinical severity classification used in teledentistry monitoring tools [9].

8.2 Regulatory Considerations

A system providing information to inform orthodontic treatment decisions would be classified as **Software as a Medical Device (SaMD)**:

- **EU MDR 2017/745:** likely Class IIa, requiring CE marking.
- **FDA:** De Novo pathway analogous to DentalMonitoring’s 2024 clearance provides regulatory precedent.
- **GDPR / HIPAA:** IOS data constitutes health data subject to enhanced privacy requirements.

Both ORTHOAI v1 and ORTHOAI v2 are scoped to *research use only*.

8.3 Limitations and Comparison with v1

Table 4 summarises limitations resolved between versions.

Table 4: Limitation comparison: v1 vs. v2.

Limitation	v1	v2
Centroid-only geometry	Yes	Resolved
Scalar quality score	Yes	Resolved
No staging simulation	Yes	Resolved
No SaaS interface	Yes	Resolved
Synthetic data only	Yes	Ongoing
Automatic movement gen.	No	Planned
Attachment placement	No	Planned

Limitations that remain open for ORTHOAI v2 include: (i) validation on real clinical IOS datasets (IOSLandmarks-1k [2], Teeth3DS [12]); (ii) automatic movement sequence generation via constrained optimisation or RL; (iii) automatic SmartForce[®] attachment placement.

9 Discussion

The transition from ORTHOAI v1 to ORTHOAI v2 illustrates a broadly applicable design pattern for clinical AI systems: *establish a working single-agent baseline with principled evaluation*, then *expand sensing coverage and decompose the scoring function*. The +21% quality gain between versions decomposes into two independent contributions of similar magnitude:

improved scoring model ($\sim+12$ pts) and agent fusion ($\sim+4.5$ pts). This decomposition has practical implications: for resource-constrained deployments where running CHARM is not feasible, upgrading only the scoring model of v1 already recovers the majority of the quality gain.

The dual-agent architecture reflects a fundamental tension in 3D dental AI: **segmentation-first** methods (Agent 1) provide geometrically precise individual tooth models but propagate segmentation errors downstream; **landmark-first** methods (Agent 2) are faster and more robust to incomplete dentitions but yield less granular geometric information. The sequential orchestration mode resolves this tension for the majority of cases (complete dentitions, mild-to-moderate crowding), invoking Agent 1 only where CHaRM confidence falls below threshold.

Looking forward, ORTHOAI v2 SaaS provides the infrastructure for a prospective pilot study at CHU de Lille’s orthodontic department: four preset cases represent the primary clinical archetypes encountered in an Invisalign caseload (Class I crowding, open bite, diastema, Class II), and the checklist module operationalises the pre-approval workflow for direct clinical usability assessment.

10 Conclusion

We presented ORTHOAI v2, a systematic extension of our prior single-agent framework [1] for open-source AI-assisted orthodontic treatment planning. The three principal contributions—dual-agent fusion, composite biomechanical scoring, and multi-frame staging simulation—collectively lift planning quality from 76.4 ± 8.3 to 92.8 ± 4.1 on our synthetic benchmark, reduce score variance by 53%, and improve treatment feasibility from 78% to 89%, while maintaining full CPU deployability and adding a production-grade SaaS interface.

Three directions define the path to **v3**: (1) prospective validation on real clinical IOS datasets, leveraging the 3DTeethLand MICCAI 2024 benchmark and CHU de Lille’s scan archive; (2) automatic movement sequence generation via constrained optimisation or multi-step reinforcement learning; (3) SmartForce[®]-analogous attachment placement and staging recommendation to reach clinical-grade decision support.

Source code and SaaS deployment package: <https://github.com/edouard-lansiaux/orthoai-v2>

Acknowledgements

The author thanks the STaR-AI Research Group (CHU de Lille) for clinical feedback on the scoring model, the organisers of the 3DTeethLand MICCAI 2024 challenge for the Teeth3DS benchmark, and the authors of CHaRM [2] for their detailed methodology description.

References

- [1] E. Lansiaux, M. Leman, M Ammi. ORTHOAI v1: A single-agent point-cloud pipeline for AI-assisted orthodontic treatment planning with clear aligners. *arXiv:2603.00124*, March 2026. <https://arxiv.org/abs/2603.00124>
- [2] J. Rodríguez-Ortega, F. Pérez-Hernández, and S. Tabik. CHARM: Conditioned heatmap regression methodology for accurate and fast dental landmark localization. *arXiv:2501.13073v5*, 2025.
- [3] Y. Wang, Y. Sun, Z. Liu, S. E. Sarma, M. M. Bronstein, and J. M. Solomon. Dynamic graph CNN for learning on point clouds. *ACM Transactions on Graphics*, 38(5):1–12, 2019.
- [4] T.-H. Wu, C. Lian, S. Lee, M. Pastewait, et al. Two-stage mesh deep learning for automated tooth segmentation and landmark localization on 3D intraoral scans. *IEEE Transactions on Medical Imaging*, 41(11):3158–3166, 2022.
- [5] B. Baquero, M. Gillot, L. Cevidanes, et al. Automatic landmark identification on intraoral scans. In *Workshop on Clinical Image-Based Procedures*, pages 32–42. Springer, 2022.
- [6] C. Lian, L. Wang, T.-H. Wu, et al. Deep multi-scale mesh feature learning for automated labeling of raw dental surfaces from 3D intraoral scanners. *IEEE Transactions on Medical Imaging*, 39(7):2440–2450, 2020.
- [7] J. Im, J.-Y. Kim, H.-S. Yu, et al. Accuracy and efficiency of automatic tooth segmentation in digital dental models using deep learning. *Scientific Reports*, 12(1):9429, 2022.
- [8] M. Yamagata, K. Hotta, H. Shimizu, et al. DilatedToothSegNet: Tooth segmentation network on 3D dental meshes. *Journal of Imaging Informatics in Medicine*, 2024.

- [9] G. E. Carlsson, L. Andersson, J. Bjerklin, et al. Artificial intelligence for orthodontic diagnosis and treatment planning: A scoping review. *Journal of Dentistry*, 150:105222, 2024.
- [10] R. Li, Q. Chen, and W. Zhang. Unveiling the role of AI applied to clear aligner therapy: A scoping review. *Journal of Dentistry*, 153:105–115, 2025.
- [11] H. Woo, C. Jung, and K.-H. Kim. Automatic virtual setup for orthodontic treatment planning using deep learning. *Scientific Reports*, 10:20738, 2020.
- [12] A. Ben-Hamadou, N. Neifar, A. Rekik, et al. Teeth3DS+: An extended benchmark for intraoral 3D scans analysis. *arXiv:2210.06094*, 2022.
- [13] B. Glaser. *The Insider’s Guide to Invisalign Treatment*. Independent, 2017. ISBN: 9780996677677.
- [14] N. D. Kravitz, B. Kusnoto, E. BeGole, A. Obrez, and B. Agran. How well does Invisalign work? A prospective clinical study evaluating the efficacy of tooth movement with Invisalign. *American Journal of Orthodontics and Dentofacial Orthopedics*, 135(1):27–35, 2009.
- [15] W. R. Proffit, H. W. Fields, D. M. Sarver, and J. L. Ackerman. *Contemporary Orthodontics*, 6th ed. Elsevier Mosby, 2018.
- [16] Align Technology. ClinCheck Live Plan: Automated treatment planning launch. Technical Report, October 2025. <https://www.aligntech.com>
- [17] E. Lansiaux, M. Leman Intelligence artificielle appliquée à la planification de traitement orthodontique par aligneurs transparents: Revue de littérature et état de l’art industriel. Working document, CHU de Lille / Université de Lille, February 2026.